Ashok Kumar*, Deepam Maurya, Yuan Zhou, Jonathan Metzman, James R. Heflin, Robert Bodnar and Shashank Priya*

Opto-electrical Behavior of $Pb(Zn_{1/3}Nb_{2/3})O_3$–$Pb_{0.97}La_{0.03}(Zr,Ti)O_3$ Transparent Ceramics with Varying Defect Structure

Abstract: We report correlation between the electromechanical, ferroelectric, optical and opto-electric behavior in $Pb(Zn_{1/3}Nb_{2/3})O_3$–$Pb_{0.97}La_{0.03}(Zr,Ti)O_3$ transparent ceramics. Optical interaction during current–voltage (I–V) measurements enhanced the current output and revealed its strong dependence on wavelength and power of the impinging radiation. Piezoresponse force microscopy revealed that the improved characteristics at low stoichiometric excess of various elements were related to nano-sized stripe domains. Raman analysis indicated the presence of short-range clusters with rhombohedral–tetragonal phase distributed at much above the Curie temperature. The results reveal the potential of these ceramics in wireless opto-electric devices operating over a wide-range of wavelengths and temperatures. These classes of ceramics have successfully demonstrated in literature for use in pyroelectric generators and UV light energy harvesting, piezoelectric transformers.

Keywords: piezoelectrics, transparent ceramics, ferroelectric, opto-electric, electromechanical

DOI 10.1515/ehs-2014-0018

***Corresponding authors: Ashok Kumar:** E-mail: ashokku@vt.edu, **Shashank Priya:** E-mail: spriya@vt.edu, Center for Energy Harvesting Materials and Systems (CEHMS), Bio-inspired Materials and Devices Laboratory (BMDL), Virginia Tech, Blacksburg, VA 24061, USA
Deepam Maurya: E-mail: mauryad@vt.edu, **Yuan Zhou:** E-mail: yzhou6@vt.edu, Center for Energy Harvesting Materials and Systems (CEHMS), Bio-inspired Materials and Devices Laboratory (BMDL), Virginia Tech, Blacksburg, VA 24061, USA
Jonathan Metzman: E-mail: metzmanj@vt.edu, **James R. Heflin:** E-mail: rheflin@vt.edu, Department of Physics, Virginia Tech, Blacksburg, VA 24061, USA
Robert Bodnar, Department of Geosciences, Virginia Tech, Blacksburg, VA 24061, USA, E-mail: rjb@vt.edu

Introduction

Lead zirconate titanate ($Pb(Zr,Ti)O_3$) (PZT), a non-centrosymmetric material obtained via solid-solution of ferroelectric $PbTiO_3$ ($T_c = 490°C$) and antiferroelectric $PbZrO_3$ ($T_c = 230°C$) compounds, has been widely used in piezoelectric and ferroelectric devices such as transducers, sensors and ferroelectric random access memory. In modified form, this material is revolutionizing applications ranging from medical ultrasound and sonar to energy harvesting (Cohen 2006; Ahart et al. 2008; Cowley et al. 2011). Recent investigations have focused on the development of PZT-based high-performance relaxor modified compositions as exemplified by the pseudo-ternary composition $Pb(Zr,Ti)O_3$–$Pb(Zn_{1/3}\ Nb_{2/3})O_3$ (PZT–PZN) system (Uchino 1997; Yin, Zhu, and Zeng 2009). Both PZN and PZT exhibit perovskite (ABO_3) lattice structure in which the A-site is occupied by Pb^{2+} ions and the B-site by Zn^{2+}, Zr^{4+}, Ti^{4+} and Nb^{5+} ions (Nonnenmann, Gallo, and Spanier 2010; Ryu et al. 2011). The solid solution of PZN–PZT has a rhombohedral/tetragonal morphotropic phase boundary (MPB) at or above ≥ 70 mol% $PbZr_xTi_{1-x}O_3$ ($0.52 \le x \le 0.54$) (He et al. 2009; Fan and Kim 2002; Wang et al. 2012). Monoclinic phases such as P_m and C_m have been reported to exist around the MPB, acting as an intermediate bridging phase that allows polarization to rotate from [111] to [001] (Ahart et al. 2008; La-Orauttapong et al. 2002; Rahman, Metselaar, and Karmaker 2014; Pandey and Singh 2014; Li and Chou 2003, 2006).

PZN ceramics exhibit good dielectric and electrostrictive properties; however, it is difficult to synthesize single phase polycrystalline perovskite PZN ceramic because steric and electrostatic interaction between high polarization of the Pb^{2+} and the Zn^{2+} cations makes it thermodynamically unstable over a wide range of temperatures (600–1,400°C). This leads to the formation of a pyrochlore phase and PbO given by the decomposition reaction [$3Pb(Zn_{1/3}Nb_{2/3})O_3 \rightarrow Pb_2Nb_2O_7 + ZnO + PbO$] (Fan and Kim 2002). The columbite method has been found to be effective in eliminating the formation of a pyrochlore

phase in some relaxor ceramics, e.g. $Pb(Mg_{1/3}Nb_{2/3})O_3$ (Haertling 1999; Wu et al. 2008). However, this method is still challenging for PZN-based ceramic systems; and PZN ceramics synthesized using these processes are opaque. Although pure PZT is opaque, lanthanum doping on the A-site has been shown to impart transparency (Zeng et al. 2005a, 2005b, 2006, 2007; Shannon, 1976; Etin et al. 2007). Hence, La incorporation in PZN–PZT ceramics has been an effective method to induce transparency and at the same time improve the dielectric, piezoelectric and opto-electric properties of compositions near the MPB.

Furthermore, La-doped $Pb(ZrTi)O_3$ (PLZT) has been used to harvest thermal energy using pyroelectric effect (Chin et al. 2012). During pyroelectric energy harvesting, system generates power from temperature fluctuations in contrast to the case of thermoelectric energy harvesting, which utilizes temperature gradient (Bowen et al. 2014). The PLZT-based epitaxial thin films on Nb-doped $SrTiO_3$ substrate, with Au/PLZT/Pt structure, has been reported to exhibit large photovoltaic output (Qin, Yao, and Liang 2010). Moreover, researchers investigated the effect of UV light on the output of the radial mode piezoelectric transformer based on PLZT (Kozielski, Adamczyk, and Erhart 2011). They reported substantial effect of UV light on efficiency and voltage step-up ratio of these piezoelectric transformers due to coupling between piezoelectricity and photostriction. Therefore, the PLZT-based materials are photoactive and can be used not only to harvest vibration energy (like other piezoelectric materials) but also can be used to harvest light and thermal energy. Other wide band materials such as zinc oxide have also been used for thermal energy harvesting (Zhao et al. 2014; Hussain et al. 2014; Feldhoff and Geppert 2014).

In this study, solid solutions of La-doped PZN–PZT ceramics with composition of $0.3Pb(Zn_{1/3}Nb_{2/3})O_3 - 0.7Pb_{0.97}La_{0.03}(Zr_xTi_{1-x})O_3$ $(0.52 \le x \le 0.54)$ have been synthesized and investigated for their electro-mechanical, ferroelectric, dielectric and opto-electrical properties. Illumination wavelength-dependent current–voltage behavior was quantified. Raman studies revealed the presence of polar nanoregions (PNRs) persisting much above the Curie temperature. The interaction of these PNRs with optical radiation in the given temperature regime could present intriguing opto-electric interactions.

Experimental details

Transparent ceramics with a composition of $0.3Pb(Zn_{1/3}Nb_{2/3})O_3–0.7Pb_{0.97}La_{0.03}(Zr_xTi_{1-x})O_3$ $(0.52 \le x \le 0.54)$ were synthesized through the solid state reaction using PbO, ZnO, Nb_2O_5, La_2O_5, ZrO_2 and TiO_2 powders. The precursor $ZnNb_2O_6$ (JCPDS # 37–1371) used for the synthesis was obtained by the solid state reaction of ZnO and Nb_2O_5. Structural analysis was conducted by x-ray diffraction with CuK_α radiation. Microstructures were observed using a scanning electron microscope (Zeiss Model Leo 1550). P–E hysteresis measurements were performed using a ferroelectric tester (Radiant Technologies Inc. Model Precision Premier II). Electromechanical coupling factor (k_p) was calculated using resonance and anti-resonance frequencies (Hewlett Packard Model 4194A) and a UV-Vis-NIR spectrophotometer (Hitachi U-4100) was used for transmittance measurements. Raman spectra were recorded in the range of 100–1,000 cm^{-1} using a Raman spectrometer (JY Horiba LabRam HR 800, Horiba Ltd., Japan) equipped with a CCD detector and a 514.5 nm argon laser of 50 mW power at the source. All samples had a Zr/Ti ratio of 0.54/0.46 and were ball milled for 48 h if not mentioned otherwise.

Results and discussion

X-ray diffraction (XRD) patterns of $0.3Pb(Zn_{1/3}Nb_{2/3})O_3–0.7Pb_{0.97}La_{0.03}(Zr_xTi_{1-x})O_3$ $(0.52 \le x \le 0.54)$ transparent ceramics are shown in Figure 1(a). These exhibit formation of a perovskite phase with or without a pyrochlore ($Pb_2Nb_2O_7$, JCPDS # 40–0828) phase, depending upon the processing duration, initial precursors and stoichiometric excess of elements such as Pb, Nb, La or Zn and/or Zr/Ti ratio. Figure 1 (a-u2) and (b-1) and (a-u16) and (b-5) shows XRD patterns of 5% stoichiometric excess of Pb at Zr/Ti ratios of 54/46 ($x = 0.54$) and 52/48 ($x = 0.52$), respectively. The excess lead revealed selective elimination of the $Pb_2Nb_2O_7$ phase, i.e. samples with a Zr/Ti ratio of 52/48 exhibited complete removal of $Pb_2Nb_2O_7$ phase. The ceramics synthesized with a Zr/Ti ratio of 54/46 exhibited reduced formation of the $Pb_2Nb_2O_7$ phase when the ball milling duration was increased to 144 h. Use of the $ZnNb_2O_6$ precursor in place of ZnO and Nb_2O_5 at the Zr/Ti ratio of 54/46 also showed reduced formation of the $Pb_2Nb_2O_7$ phase. These ceramics were further investigated for the stoichiometric excess of elements such as Nb, La and Zn. Stoichiometric excess of La and Nb showed none or negligible effect on the formation of the $Pb_2Nb_2O_7$ phase (Figure 1(a)–(b)). However, at 5% stoichiometric excess of Zn, the complete leaching of a pyrochlore phase was obtained (Figure 1(b-4)). Scanning electron micrographs of the cross-section of $0.3Pb(Zn_{1/3}Nb_{2/3})O_3–0.7Pb_{0.97}La_{0.03}(Zr_xTi_{1-x})O_3$ ceramics (figures not

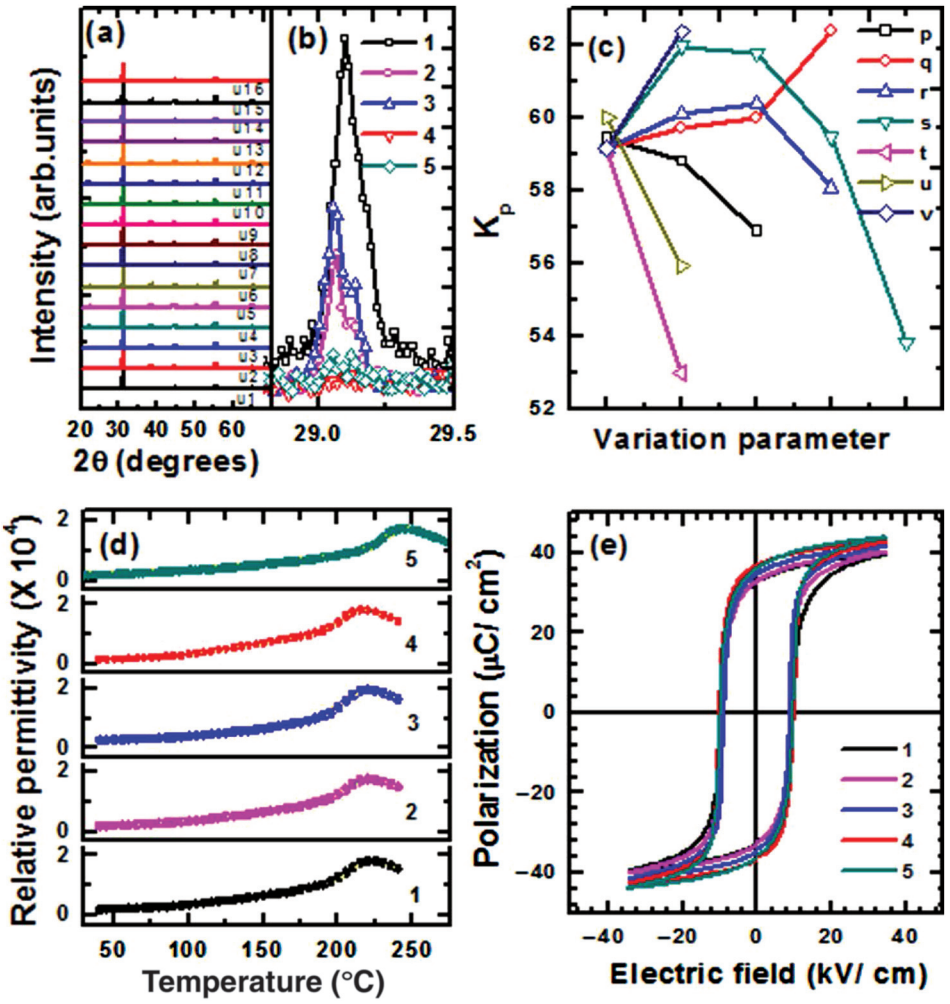

Figure 1 (Color online) (a) X-ray diffraction (XRD) patterns of $0.3Pb(Zn_{1/3}Nb_{2/3})O_3–0.7Pb_{0.97}La_{0.03}(Zr_xTi_{1-x})O_3$ ($x = 0.54$) ceramics with stoichiometric excess of (u1–u3) 0, 5, 10% Pb, (u4–u6) 1.5, 2.5, 5% Nb, (u7–u9) 1.5, 2.5, 5% La, (u10–u12) 1.5, 2.5, 5% Zn, (u13) 0% Pb ball milling for 144 h, (u14) columbite method, (u15) 0% Pb with Zr/Ti ratio of 52/48 and (u16) 5% Pb with Zr/Ti ratio of 52/48 and (b) showing formation/extinction of $Pb_2Nb_2O_6$ phase, (c) variation of electromechanical coupling factor (k_p) [with excess (p) Pb, (q) Zn, (r) Nb, (s) La, (t) Pb (columbite method), (u) Pb ball milling for 144 h and (v) 5% excess Pb, Zr/Ti ratio 52/48], (d) Variation of dielectric permittivity with temperature and (e) P-E hysteresis curves for (1) 0% Pb, (2) 0% Pb-columbite method, (3) 0% Pb, ball milling for 144 h, (4) 5% Zn and (5) 5% Pb, Zr/Ti ratio 52/48

shown due to space limitations) showed high uniformity and density.

The formation of secondary phase has been attributed to the Pb deficiency, and therefore, excess Pb could lead to crystallization of pure perovskite phase. However, the complete extinction of the $Pb_2Nb_2O_7$ phase (at 5% excess stoichiometric Pb) was observed only at a Zr/Ti ratio of 52/48 (but not at Zr/Ti ratio of 54/46) and can be interpreted as follows. Zirconium (Zr) is a tetravalent ion, while titanium (Ti) can occur in the $+4$, $+3$, and $+2$ valence states. However, in this study samples were synthesized in oxygen ambient and, therefore, Ti will be mainly in Ti^{4+} state. The ionic radii of Zr^{4+} and Ti^{4+} in sixfold coordination are 0.72 and 0.605 Å, respectively (Miller, Vandome, and McBrewster 2010). Replacing Zr with Ti results in lattice contraction because of the smaller radius of Ti^{4+} compared to Zr^{4+} ions. This, in turn, may reduce the B–O bond length of ABO_3 type structure and provide stability to the perovskite structure (Zhang et al. 2006). Further, using the columbite method and increasing ball milling duration both results in reduced formation of $Pb_2Nb_2O_7$. Addition of excess ZnO has been found to stabilize the perovskite phase. Also, 5% stoichiometric excess of zinc resulted in the complete removal of the $Pb_2Nb_2O_7$ phase (Zeng et al. 2005a). Figure 1(c) shows the variation in the electro-mechanical coupling factor (k_p) as a function of stoichiometric excess of various elements and processing conditions. Increasing Pb

content reduces k_p in all samples. Samples synthesized using individual oxide powders as precursors and using the columbite method both show similar behavior of k_p with Pb excess. However, the columbite method resulted in a lower value of k_p ~53%. In lead-based piezoelectric materials, Pb vacancies are inevitable during processing at higher temperature. However, these Pb vacancies could generate oxygen vacancies according to Schottky equilibrium (null $\rightarrow V_{Pb} + V^{\circ\circ}_{O}$) to maintain local charge neutrality (Huang, Chen, and Wu 2004; Wu and Cao 1999). Niobium and lanthanum act as soft doping ions on B- and A-sites, respectively. The substitutions of Nb^{5+} on B^{4+} sites and La^{3+} on A^{2+} sites, results in extra positive charges. This extra charge could reduce the formation of oxygen vacancies due to Schottky equilibrium leaving only Pb vacancies in the system (Kubinski and Holloway 1995). These Pb vacancies have been considered to facilitate the domain wall motion resulting in high electro-mechanical response in soft piezoelectric materials (Flygare and Gierke 1974). Therefore, the increased value of k_p, in the case of excess niobium and lanthanum content could be attributed to these Pb vacancies. Moreover, excess zinc addition resulted in a continuous increase in k_p, due to reduced pyrochlore phase (Zeng et al. 2005a). The specimen processed with extended ball milling duration (144 h) resulted in higher k_p values, independent of the processing method or excess stoichiometric content of various elements. The highest values of k_p ~62.3% were observed in samples with 5% stoichiometric excess of Zn and 5% Pb (Zr/Ti ratio of 0.52/0.48).

Figure 1(d) shows the variation in dielectric permittivity with temperature in the frequency range 100 Hz–15 MHz for each sample. The dielectric permittivity variation with frequency is not significant, and, therefore, the various curves taken at different frequencies seem to overlap (Figure 1 (d)). The Curie temperature (T_c) for the stoichiometric sample synthesized at a Zr/Ti ratio of 54/46 is about 222°C. However, the sample containing 5% excess Pb exhibited T_c of 245°C at a Zr/Ti ratio of 52/48. As noted above, the ionic radii of Zr^{4+} and Ti^{4+} in sixfold coordination are 0.72 and 0.605 Å, respectively (Miller, Vandome, and McBrewster 2010). The smaller size of the Ti^{4+} ion in the octahedral site increases the rattling tendency, which, in turn, elevates the Curie temperature (Flygare and Gierke 1974). The substitution of La^{3+} and Nb^{5+} upto certain extent of concentration results in similar effect on lattice relaxation and could lead to the relaxation of oxygen framework to the tilted structure (Seinfeld and Pandis 2006). Also, there is none or negligible formation of the $Pb_2Nb_2O_7$ phase, indicating that most of the Nb^{5+} ions occupy the "B" lattice sites. The Curie temperature of $0.3Pb(Zn_{1/3}Nb_{2/3})O_3–0.7Pb_{0.97}La_{0.03}(Zr_xTi_{1-x})O_3$ ($x = 0.54$) at 0% stoichiometric excess lead content and synthesized using single oxides or $ZnNb_2O_6$ precursor processed for 48 h, is 222°C. The Curie temperature is marginally decreased (~220°C) at increased ball milling time (144 h). The sample with 5% excess stoichiometric Zn exhibited the lowest Curie temperature (217°C). Excess Zn content restricted the formation of the $Pb_2Nb_2O_7$ phase completely and, therefore, retained all the Nb^{5+} in the ABO_3 type lattice. Inserting zinc as $+2$ and Nb as $+5$ into "B" sites in an ABO_3 type structure requires charge compensation and, in turn, may reduce the formation of oxygen vacancies. Also, the larger ionic radius of Zn^{2+} (0.74 Å) in sixfold coordination in comparison to Nb^{5+} (0.64 Å) and Ti^{4+} (0.605 Å) reduces the size of rattling space and, in turn, will reduce the tendency of Zn^{2+} ions to rattle, leading to a reduced Curie temperature.

Figure 1(e) shows the polarization versus electric field (P–E) hysteresis curves for the $0.3Pb(Zn_{1/3}Nb_{2/3})O_3–0.7Pb_{0.97}La_{0.03}(Zr_xTi_{1-x})O_3$ samples. Samples with a stoichiometric composition and Zr/Ti ratio of 54/46 exhibit a saturation polarization (P_s) value of ~39.4 μC/cm^2. This value is slightly increased (~40.0 μC/cm^2) if the samples were synthesized using $ZnNb_2O_6$ precursor. Increased ball milling duration of precursors (~144 h) resulted in a further increase in the P_s value (~41.6 μC/cm^2) due to reduced formation of secondary phase. An excess stoichiometric content of 5% Zn increased P_s values further to 42.5 μC/cm^2. The samples with 5% excess stoichiometric lead content at $x = 0.52$ exhibited the highest P_s values of 43.6 μC/cm^2. Furthermore, the stoichiometric $0.3Pb(Zn_{1/3}Nb_{2/3})O_3–0.7Pb_{0.97}La_{0.03}(Zr_xTi_{1-x})O_3$ sample was found to exhibit coercive field (E_c) ~9.49 kV/cm. This value is slightly decreased in the samples prepared using the columbite method (9.1 kV/cm). Ball milling of the samples for longer durations, i.e. up to 144 h, further reduced the coercive field to 8.76 kV/cm. The values of E_c for 5% excess Pb (Zr/Ti ratio 52/48) and 5% Zn were found to be 9.7 and 9.9 kV/cm, respectively.

Figure 2(a) shows the optical transmittance of the $0.3Pb(Zn_{1/3}Nb_{2/3})O_3–0.7Pb_{0.97}La_{0.03}(Zr_xTi_{1-x})O_3$ samples. The samples with 5% excess stoichiometric zinc content at $x = 0.54$ exhibited the highest transmittance in the visible region followed by the transmittance of the samples containing 5% excess lead at $x = 0.52$ (the transmittance values of the samples with 5% excess lead at $x = 0.52$ were highest above a wavelength of 800 nm). The transmittance (T) values for other samples increased according to the relation: samples synthesized using individual oxides < samples synthesized using the columbite

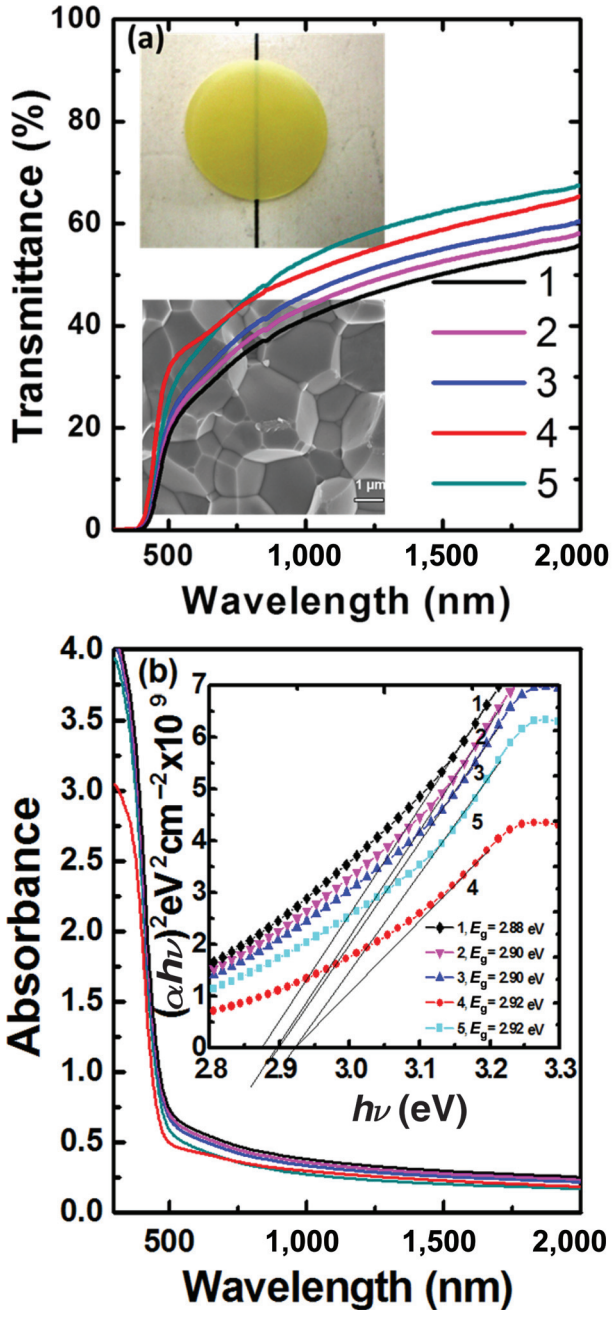

Figure 2 (Color online) (a) Transmittance in the wavelength range 300–2,000 nm; insets show transmittance image of a line through a typical sample of thickness 0.35 mm, and its photomicrograph, and (b) UV-Vis-NIR absorbance spectra for the $0.3Pb(Zn_{1/3}Nb_{2/3})O_3$–$0.7Pb_{0.97}La_{0.03}(Zr_xTi_{1-x})O_3$ ($x = 0.54$) samples with excess (1) 0% Pb, (2) 0% Pb-columbite method, (3) 0% Pb ball milling for 144 h, (4) 5% Zn and (5) 5% Pb, Zr/Ti ratio 52/48, respectively

method < samples synthesized with extended ball milling time of 144 h. The T values for these samples were smaller than those of the samples synthesized using 5% excess Zn content and/or 5% excess Pb (at Zr/Ti ratio of 52/48). Insets in Figure 2(a) show the transmittance image and a photomicrograph of a typical sample. Microstructural variables such as density, grains size, microscopic pores, point defects and secondary phase modify the transmittance behavior (Hu et al. 2010). The poor transmittance value in pyrochlore containing sample can be attributed to the increased scattering through its segregation at grain boundaries. Also, the progressive increase in transmittance value with increase in wavelengths results due to grain size and wavelength-dependent scattering effects (Wang 2010).

The variation of optical absorbance as a function of wavelength, where h denotes Planck constant and ν is the frequency of radiation, is shown in Figure 2(b). The absorbance data were obtained in transmission mode for the sample thickness of 0.35 mm (for each sample). The variation of $(\alpha h\nu)^2$ as a function of energy ($h\nu$), where α is the absorption coefficient, is displayed in the inset of Figure 3(b). The band gap energy E_g is obtained by extrapolating the linear portion of the graph to energy axis at $\alpha = 0$. The optical band gap (E_g) estimated using the relation, $(\alpha h\nu) = C(h\nu - E_g)^n$, where C is the constant and $n = ½$ for a direct allowed transition, were 2.88, 2.90, 2.90, 2.92, and 2.92 eV for the samples with excess (1) 0% Pb, (2) 0% Pb-columbite method, (3) 0% Pb ball milling for 144 h, (4) 5% Zn and (5) 5% Pb, Zr/Ti ratio 52/48, respectively. Chemistry at A- and B- sites, more specifically, the ionic sizes modify the band gap (Wang 2010). However, the B–O bonding characteristics predominates the optical band-gap over A-site chemistry. In the present study, the higher band gap values in the case of 5% excess Zn (Zr/Ti ratio 54/46) and 5% excess Pb (Zr/Ti ratio of 52/48) can be attributed to the increased content of larger size ions, i.e. Zn^{2+} (0.74 Å) and Zr^{4+} (0.72 Å) at B sites. Since, $0.3Pb(Zn_{1/3}Nb_{2/3})O_3$–$0.7Pb_{0.97}La_{0.03}(Zr_xTi_{1-x})O_3$ ($x = 0.54$) ceramics at the stoichiometric excess of 5% Zn exhibit the highest optical band gap and transmittance (in the visible range), these ceramics were further investigated to examine their current–voltage behavior to identify their possible applications in electro-optical-devices.

The low stoichiometric excess of all elements, e.g. Nb, La and Zn in $0.3Pb(Zn_{1/3}Nb_{2/3})O_3$–$0.7Pb_{0.97}La_{0.03}(Zr_xTi_{1-x})O_3$ ($x = 0.54$), revealed the improved characteristics. To understand its relation with domain shape, size and orientation, we investigated two samples; one of stoichiometric composition (sample code S1) and other with 1.5% stoichiometric excess of Nb (sample code S2) using Piezoresponse force microscopy (PFM, Dimension Icon, Bruker). Figure 3 (a)–(d) shows the PFM phase and amplitude mapping of samples S1 and S2 respectively (of approximately 100 μm thickness). It was noticed that all the piezoreponse images exhibited a strong domain

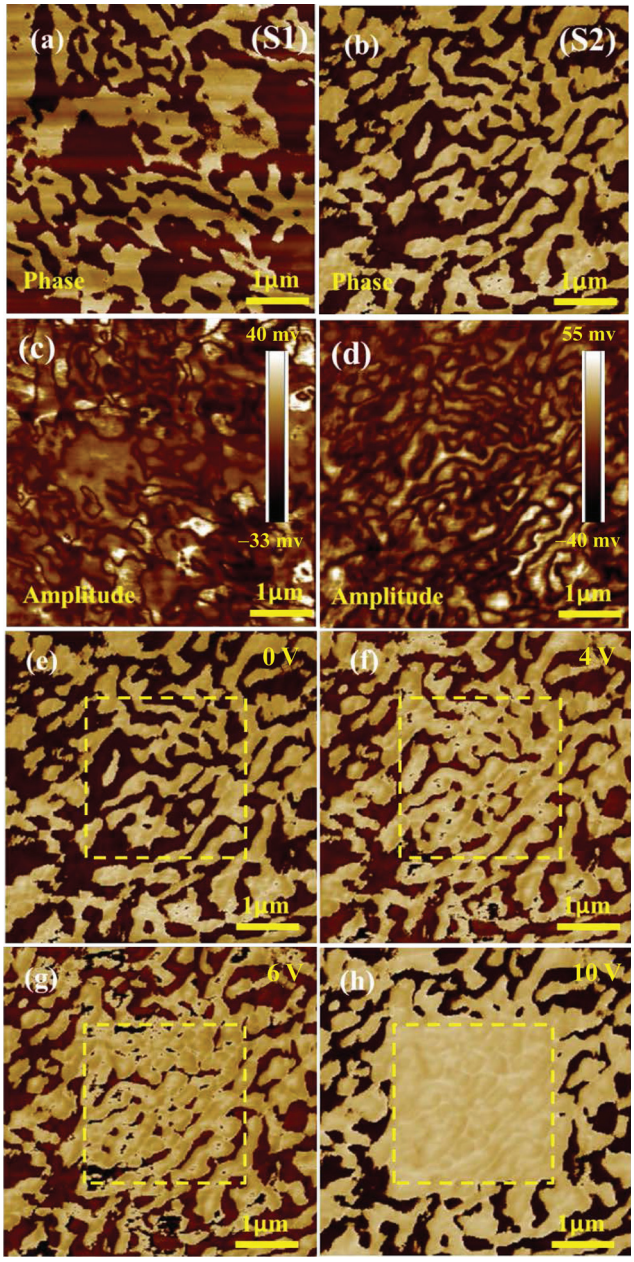

Figure 3 (Color online) shows the PFM images of phase (a, b) and amplitude (c, d) mapping for $0.3Pb(Zn_{1/3}Nb_{2/3})O_3–0.7Pb_{0.97}La_{0.03}(Zr_{0.54}Ti_{0.46})O_3$ (sample code S1) and with stoichiometric excess of 1.5% Nb (sample code S2); (e, f, g and h) show the PFM images of phase mapping for S2 with varying poling voltages

contrast: deep bright and dark areas indicating significant out-of-plane component of polarization. We further observed that along with the decrease in size, domains themselves became more oriented for the specimen with stoichiometric excess of 1.5% Nb. Nano-sized strip domains with size ~100–200 nm were found in the sample S2. The piezoelectric response has been considerably found to depend on the domain sizes as the systems with easily switchable nano-sized domains could exhibit a large improvement in functional response. The field-induced polarization transition in S2 sample is explored through the polarization switching experiments (Figure 3 (e)–(h)). Prior to PFM characterization, square polarization pattern (2.5 μm × 2.5 μm) was generated in the sample by scanning the surface with an applied dc bias voltage of 0 V, +4 V, +6 V and +10 V, respectively. The enlarged bright contrast of the phase image before and after the application of electric field confirms the strong polarization switching in the sample. In the absence of external electric field, the strip bright/dark contrast is uniform. After the application of external electric field, the corresponding polarization dramatically increased with deep bright area, due to reversal in polarization orientation. Meanwhile, PFM amplitude images taken at each voltage step exhibit a uniform contrast, with the polarized-square pattern amplitude steadily increasing with each incremental step. The depolarization field, due to presence of these ferroelectric domains having different polarization, could facilitate the separation of photo-generated charge carriers modulating the electrical output of the system.

Figure 4(a) shows the spectral dependence of the current–voltage (I–V) curves of a typical $0.3Pb(Zn_{1/3}Nb_{2/3})O_3–0.7Pb_{0.97}La_{0.03}(Zr_xTi_{1-x})O_3$ ($x = 0.54$) ceramic at the stoichiometric excess of 1.5% Nb. The current varies as a function of illumination wavelength; and the illumination of the sample with the shorter wavelength radiation exhibits higher current density. Obviously, the value of current density at 300 nm radiation is higher than of 700 nm, though the lamp profile shows comparative higher power at 700 nm. This is mainly because of high absorbance of the sample at 300 nm than at 700 nm (Figure 2(b)). The value of current density at 500 nm is higher than of 300 nm due to strong power of lamp at 500 nm. In Figure 4(a) these samples were illuminated with xenon lamp, which, in turn, has lower irradiance in comparison to laser light (Figure 4(b)). Figure 4(b) shows the I–V curves obtained in dark (before light interaction), by illumination of the sample with 530 nm laser light, and in dark (after light interaction), respectively. Obviously, the laser (530 nm) light exhibits larger change in the value of current in comparison to the lamp light. The dark current measurements performed after illumination study matches well with the curve collected before measurements (inset Figure 4(a)). The mechanism of light interaction may be interpreted as follows. For piezoelectric materials, recently, it has been proposed that the stress can lead to change in local electronic band structure and cause its tilt (Seinfeld and Pandis 2006; Hu et al. 2010).

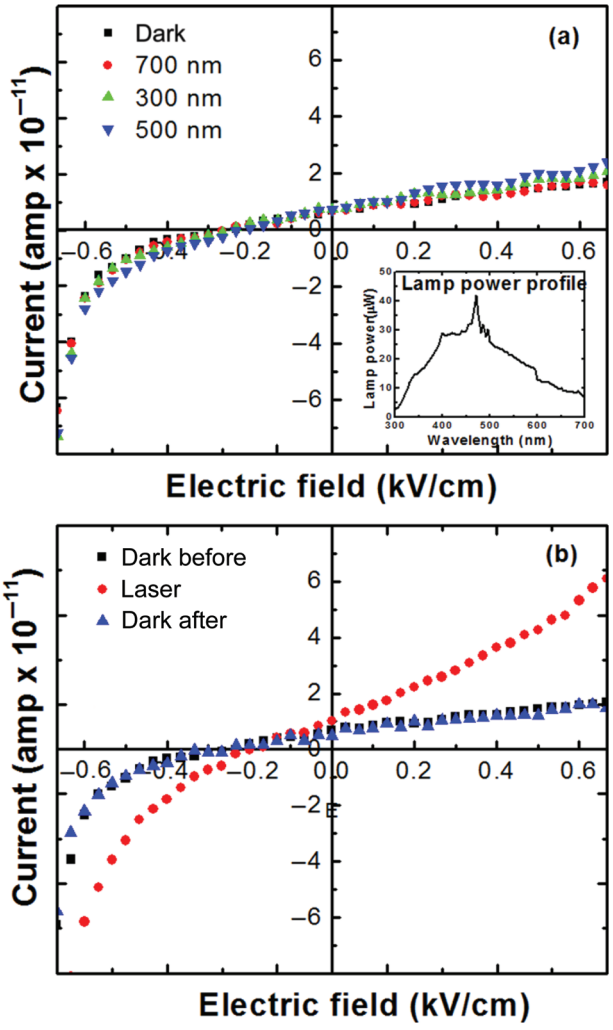

Figure 4 (Color online) Current–voltage (I–V) curve of $0.3Pb(Zn_{1/3}Nb_{2/3})O_3$–$0.7Pb_{0.97}La_{0.03}(Zr_xTi_{1-x})O_3$ ($x = 0.54$) ceramic at 1.5% stoichiometric excess Nb, using various wavelengths obtained from the lamp (a), and laser light of wavelength 530 nm (b); both (a) and (b) include a dark current curve for comparison

The 10% tensile stress in zigzag boron nitride nanoribbons was found to reduce the band gap energy value from 3.5 eV to 1.0 eV (Qi et al. 2012). Thus, the applied voltage during the I–V measurement may lower the band-gap energy slightly at the +ve potential (tensile stress) and increased at –ve (compressive stress), which, subsequently, will lead to light interacting charge recombination device similar to P–N junction (Qi et al. 2012). The other possible contributions of current may be due to heating through absorbed light, and the interaction of radiation with crystal lattice and generation of electric dipoles (though transmitted light).

To examine the effect of temperature and suitability of such devices, if operated in extreme conditions, we collected laser Raman spectra of the sample $0.3Pb(Zn_{1/3}Nb_{2/3})O_3$–

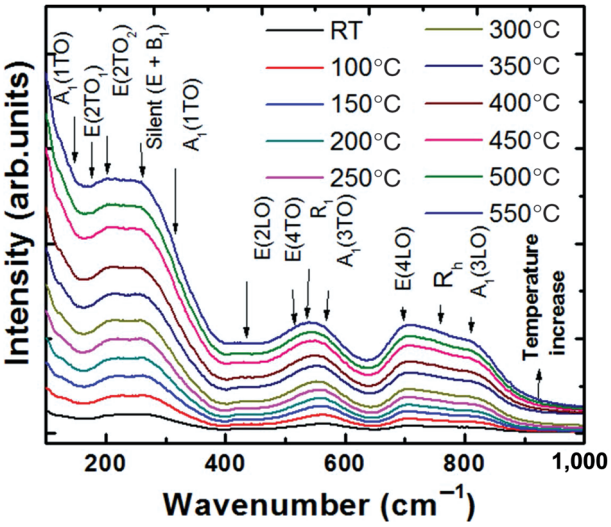

Figure 5 (Color online) Temperature-dependent Raman spectra of $0.3Pb(Zn_{1/3}Nb_{2/3})O_3$–$0.7Pb_{0.97}La_{0.03}(Zr_xTi_{1-x})O_3$ ($x = 0.54$) ceramic at the stoichiometric excess of 5% Zn

$0.7Pb_{0.97}La_{0.03}(Zr_xTi_{1-x})O_3$ ($x = 0.54$) having stoichiometric excess of 5% Zn. In Figure 5, the Raman modes R_h, R_1 and E ($2TO_2$) correspond to the R3m structure (rhombohedral), modes A_1(1TO), A_1(3LO), E(4LO), A_1(3TO), E(4TO) and E ($2TO_1$) appear due to P4mm (tetragonal) structure, and modes E(2LO), A_1(2TO) and Silent ($E + B_1$) are caused by both R3m and P4mm structures. Clearly, the sample consists of a MPB phase with rhombohedral and tetragonal structure and a total of 12 Raman modes (He et al. 2009; Fan and Kim 2002; Wang et al. 2012; La-Orauttapong et al. 2002; Rahman, Metselaar, and Karmaker 2014; Pandey and Singh 2014). These samples were further investigated as a function of temperature. Interestingly, the soft transverse modes A_1 (1TO) were present at higher temperature than the macroscopic transition temperature and exhibited a redshift in frequency with increase in temperature. Appearance of these phonon modes at higher temperature than the macroscopic transition temperature indicates order–disorder type transition due to the presence of PNRs with rhombohedral–tetragonal phases (similar features can also be observed in E phonon modes) (Zhang et al. 2011). The localized PNRs observed at higher temperatures may have different nature of interaction with optical radiation (than observed at room temperature Figure 3) and, in turn, could lead to intriguing opto-electric-interactions.

Conclusions

In conclusion, stoichiometric excess Pb, Nb, La and Zn revealed variable effects on properties. Improved properties

were noticed in stoichiometric excess of (i) 5% Zn at Zr/Ti ratio of 54/46 and (ii) 5% Pb at Zr/Ti ratio of 52/48. At lower excess stoichiometric content of various elements, the reduced domain size and their ordering contributed toward improved properties. The results of this study will lead to synthesis of materials with superior electro-mechanical, ferroelectric, dielectric, optical, opto-electrical properties for applications in wireless opto-electric-devices working over a wide range of temperatures.

Research funding: This work was supported by the Office of Basic Energy Sciences, Department of Energy through the grant number DE-FG02-06ER 46290.

References

Ahart, M., M. Somayazulu, R. E. Cohen, P. Ganesh, P. Dera, H. -K. Mao, R. J. Hemley, Y. Ren, P. Liermann, and Z. Wu. 2008. "Origin of morphotropic phase boundaries in ferroelectrics." *Nature* 451:545.

Bowen, C. R., J. Taylor, E. LeBoulbar, D. Zabek, A. Chauhan, and R. Vaish. 2014. "Pyroelectric materials and devices for energy harvesting applications." *Energy & Environmental Science* 7: 3836

Chin, T. K., F. Y. Lee, I. M. McKinley, S. Goljahi, C. Lynch, and L. Pilon. 2012. "Pyroelectric waste heat energy harvesting using 9.5/65/35 PLZT ceramics." *IEEE Transactions on Ultrasonics Ferroelectrics* 59:2373.

Cohen, R. E. 2006. "Materials science: Relaxors go critical." *Nature* 441:941.

Cowley, R. A., S. N. Gvasaliya, S. G. Lushnikov, B. Roesslic, and G. M. Rotaru. 2011. "Relaxing with relaxors: a review of relaxor ferroelectrics." *Advanced Physics* 60:229.

Etin, A., G. E. Shter, R. Brener, S. Baltianski, and G. S. Grader. 2007. "Surface Composition and Imprint in CSD-Based PZT Films." *Journal of the American Ceramic Society* 90:3800.

Fan, H., and H. E. Kim. 2002. "Perovskite stabilization and electro-mechanical properties of polycrystalline lead zinc niobate – lead zirconate titanate." *Journal of Applied Physics* 91:317.

Feldhoff, A., and B. Geppert. 2014. "A High-temperature thermo-electric generator based on oxides." *Energy Harvesting and Systems* 1:69–78.

Flygare, W. H., and T. D. Gierke. 1974. "Light Scattering in Noncrystalline Solids and Liquid Crystals." *Annual Review of Materials Research* 4:255.

Haertling, G. H. 1999. "Ferroelectric Ceramics: History and Technology." *Journal of the American Ceramic Society* 82:797.

He, X., X. Zeng, X. Zheng, P. Qiu, W. Cheng, and A. Ding. 2009. "Fabrication and characteristics of relaxor ferroelectric PZN–PZT (53/47) thin films by a MOD process." *Journal of Physics: Conference Series* 152:012068.

Hu, Y., Y. Chang, P. Fei, R. L. Snyder, and Z. L. Wang. 2010. "Transport Characteristics of ZnO Micro/Nanowire Devices by Coupling Piezoelectric and Photoexcitation Effects." *ACS Nano* 4:1234.

Huang, C. -L., B. -H. Chen, and L. Wu. 2004. "Variability of impurity doping in the modified Pb(Zr,Ti)O3 ceramics of type ABO3." *Solid State Communications* 130:19.

Hussain, M., M. A. Abbasi, A. Khan, O. Nur, and M. Willander. 2014. "Comparative Study of Energy Harvesting from ZnO Nanorods Using Different Flexible Substrates." *Energy Harvesting and Systems* 1:19–26.

Kozielski, L., M. Adamczyk, and J. Erhart. 2011. "PLZT-based photo-voltaic Piezoelectric Transformer with light feedback." *IOP Conference Series* 18:092001.

Kubinski, D. J., and H. Holloway. 1995. "Dependence of giant mag-netoresistance on the number of valence-electrons in the ferromagnetic constituent of granular alloys – precipitatesof face-centered-cubic Fe-Co, Co-Ni, and Ni-Cu alloys in Ag matrices." *Journal of Applied Physics* 77:2508.

La-Orauttapong, D., B. Noheda, Z. -G. Ye, P. M. Gehring, J. Toulouse, D. E. Cox, and G. Shirane. 2002. "Phase diagram of the relaxor ferroelectric (1-x)Pb(Zn1/3Nb2/3)O3–xPbTiO3." *Physical Review B* 65:144101.

Li, C. -L., and C. -C. Chou. 2003. "Preparation of PZN-Based Ceramics Using a Sequential Mixing Columbite Method." *Integrated Ferroelectrics* 55:955.

Li, C. -L., and C. -C. Chou. 2006. "Microstructures and electrical properties of lead zinc niobate – lead titanate – lead zirconate ceramics using microwave sintering." *Journal of the European Ceramic Society* 26:1237.

Miller, F. P., A. F. Vandome, and J. McBrewster. 2010. *Kroger-Vink Notation*. Germany: VDM Verlag Dr. Mueller GmbH & Co. KG.

Nonnenmann, S. S., E. M. Gallo, and J. E. Spanier. 2010. "Redox-based resistive switching in ferroelectric perovskite nanotubes." *Applied Physics Letters* 97:102904.

Pandey, R., and A. K. Singh. 2014. "Presence of a monoclinic (Pm) phase in the morphotropic phase boundary region of multi-ferroic (1–x)Bi(Ni1/2Ti1/2)O3-xPbTiO3 solid solution: A Rietveld study." *Applied Physics* 116:044102.

Qi, J., X. Qian, L. Qi, J. Feng, D. Shi, and J. Li. 2012. *Nano Letters* 12:1224.

Qin, M., K. Yao, and Y. C. Liang. 2010. "Development of low-cost ferroelectric PLZT devices for photovoltaic power generation." *IEEE Sustainable Energy Technology* 1:1.

Rahman, M. M., H. S. C. Metselaar, and P. C. Karmaker. 2014. "Nanoscale domain structures in 0.91Pb(Zn1/3Nb2/3)O3-0.09PbTiO3 (91PZN-9PT) single crystals studied by piezore-sponse forcemicroscopy." *Phase Transformation* 87:419.

Ryu, J., W. -H. Yoon, J. -J. Choi, B. -D. Hahn, J. -W. Kim, D. -S. Park, C. -W. Ahn, S. Priya, and D. -Y. Jeong. 2011. "Stress-controlled Pb(Zr0.52Ti0.48)O3 thick films by thermal expansion mismatch between substrate and Pb(Zr0.52Ti0.48)O3 film." *Journal of Applied Physics* 110:124101.

Seinfeld, J. H., and S. N. Pandis. 2006. *Atmospheric Chemistry and Physics*. Hoboken, NJ: John Wiley and Sons.

Shannon, R. D. 1976. "Revised effective ionic radii and systematic studies of interatomic distances in halides and chalcogenides." *Acta Crystallography A* 32:751.

Uchino, K. 1997. *Piezoelectric Actuators and Ultrasonic Motors*. Norwell, MA: Kluwer Academic.

Wang, Z. L. 2010. "Piezopotential gated nanowire devices: Piezotronics and piezo-phototronics." *Nano Today* 5:540.

Wang, N., Q. Sun, W. Ma, Y. Zhang, and H. Liu. 2012. "Investigation of La-doped 0.25Pb(Zn1/3Nb2/3)O3-0.75Pb(ZrxTi1-x)O3 ceramics near morphotropic phase boundary." *Journal of Electroceramics* 28:15.

Wu, Y., and G. Cao. 1999. "Enhanced ferroelectric properties and lowered processing temperatures of strontium bismuth niobates with vanadium doping." *Applied Physics Letters* 75:2650.

Wu, Y. J., J. Li, X. M. Chen, R. Kimura, and K. Kakegawa. 2008. "Transparent PbZrO3-PbTiO3-Pb(Zn1/3Nb2/3)O3 ceramics modified with La2O3 and PbO." *Journal of the American Ceramic Society* 91:13.

Yin, Q., B. Zhu, and H. Zeng. 2009. *Microstructure, Property and Processing of Functional Ceramics*. New York:Springer.

Zeng, X., A. L. Ding, G. C. Deng, T. Liu, and X. S. Zheng. 2005a. "Effects of lanthanum doping on the dielectric, piezoelectric properties and defect mechanism of PZN–PZT ceramics prepared by hot pressing." *Physica Status Solidi A* 202:1854.

Zeng, X., A. L. Ding, T. Liu, G. C. Deng, and X. S. Zheng. 2005b. "Excess ZnO addition in PZN–PLZT ceramics." *Physica Status Solidi A* 202:1842.

Zeng, X., A. L. Ding, T. Liu, G. C. Deng, X. S. Zheng, and W. X. Cheng. 2006. "Excess ZnO Addition in Pure and La-Doped PZN–PZT Ceramics." *Journal of the American Ceramic Society* 89:728.

Zeng, X., A. L. Ding, X. S. Zheng, and T. Liu. 2007. "Effects of excess ZnO addition on La-doped PZN–PZT ceramics prepared by hot pressing." *Ceramics International* 33:883.

Zhang, Z., L. Lu, C. Shu, and P. Wu. 2006. "Computational investigation of B-site donor doping effect on fatigue behavior of lead zirconate titanate." *Applied Physics Letters* 89:152909.

Zhang, N., H. Yokota, A. M. Glazer, and P. A. Thomas. 2011. "The not so simple cubic structure of PbZr(1-x)Ti(x)O3 (PZT): complex local structural effects in perovskites." *Acta Crystallographica B* 67:461.

Zhao, Y., A. Kumar, G. A. Khodaparast, A. Eltahir, H. Wang, and S. Priya. 2014. "Sintering temperature-dependent chemical defects and the effect on the electrical resistivity of thermoelectric ZnO." *Energy Harvesting and Systems* 1:113–19.